Technical Report 441

A. E. E. Rogers

Spectral Line Interferometry and Interferometer Noise Analysis

16 January 1968

Prepared under Electronic Systems Division Contract AF 19(628)-5167 by

Lincoln Laboratory
MASSACHUSETTS INSTITUTE OF TECHNOLOGY
Lexington, Massachusetts

The work reported in this document was performed at Lincoln Laboratory, a center for research operated by Massachusetts Institute of Technology, with the support of the U.S. Air Force under Contract AF 19(628)-5167.

MASSACHUSETTS INSTITUTE OF TECHNOLOGY
LINCOLN LABORATORY

SPECTRAL LINE INTERFEROMETRY AND INTERFEROMETER NOISE ANALYSIS

A. E. E. ROGERS

Group 31

TECHNICAL REPORT 441

16 JANUARY 1968

LEXINGTON MASSACHUSETTS

ABSTRACT

The theory of spectral line interferometry is developed with special reference to interferometer systems built to study the emission from interstellar OH molecules. Expressions for the root-mean-square noise of visibility amplitude and phase are derived in terms of the geometric means of the system and antenna temperatures. Methods are discussed for obtaining the visibility function from measurements made at widely separated sites by means of precise frequency and time standards.

Accepted for the Air Force
Franklin C. Hudson
Chief, Lincoln Laboratory Office

CONTENTS

SPECTRAL LINE INTERFEROMETRY AND INTERFEROMETER NOISE ANALYSIS

I. INTRODUCTION

The detection[1] of 18-cm radiation from interstellar OH molecules has shown the need for adding the frequency dimension to interferometry. Because of the inability of large parabolic antennas, such as the NRAO 140-foot antenna and the 210-foot antenna in Australia, to resolve the 18-cm spectral lines, several spectral line interferometers have been built to measure the spatial distribution of OH emission.[2-4] Basically, spectral line interferometry is no different from conventional interferometry in which no frequency analysis is performed; however, the spectral line interferometer is more versatile than the more conventional interferometer and has led to some improvements in conventional interferometry. In particular, the high-speed computers and digital processors used in spectral analysis are easily adapted to perform fringe rotation and delay compensation as well as the spectral analysis.

II. PRINCIPLES OF INTERFEROMETRY

Fourier theory relates the time domain electric field $\vec{E}(\vec{r}, t)$ to its Fourier components $\vec{E}(\vec{r}, \omega)$ in the frequency domain by the Fourier integrals

$$\vec{E}(\vec{r}, t) = \int \vec{E}(\vec{r}, \omega)\, e^{i\omega t}\, \frac{d\omega}{2\pi} \tag{II-1}$$

$$\vec{E}(\vec{r}, \omega) = \int \vec{E}(\vec{r}, t)\, e^{-i\omega t}\, dt \quad . \tag{II-2}$$

In an exactly analogous way, the Fourier component $\vec{E}(\vec{r}, \omega)$ can be decomposed into spatial components $\vec{E}(\vec{k}, \omega)$ where each spatial component is a plane wave

$$\mathrm{Re}\left\{\vec{E}(\vec{k}, \omega)\, e^{i\omega t - i\vec{k}\cdot\vec{r}}\right\} \tag{II-3}$$

so that

$$\vec{E}(\vec{r}, \omega) = \iint \vec{E}(\vec{k}, \omega)\, e^{-i\vec{k}\cdot\vec{r}}\, \frac{dk_x dk_y}{(2\pi)^2} \tag{II-4}$$

and

$$\vec{E}(\vec{k}, \omega) = \iint \vec{E}(\vec{r}, \omega)\, e^{i\vec{k}\cdot\vec{r}}\, dr_x dr_y \quad . \tag{II-5}$$

Integration over only two dimensions is necessary as

$$|\vec{k}| = \frac{\omega}{c} \tag{II-6}$$

thus, only two components of $\vec{k}$ are independent.

Theorems of the Fourier theory of time functions carry over into the two-dimensional Fourier theory of plane waves. The relation of the power spectral density $\vec{S}(\vec{r}, \omega)$ to the autocorrelation function $\langle \vec{E}(\vec{r}, t) \times \vec{H}^*(\vec{r}, t - \tau) \rangle_T$

$$\vec{S}(\vec{r}, \omega) = \vec{E}(\vec{r}, \omega) \times \vec{H}^*(\vec{r}, \omega) = \int \langle \vec{E}(\vec{r}, t) \times \vec{H}^*(\vec{r}, t - \tau) \rangle_T \, e^{-i\omega\tau} \, d\tau \tag{II-7}$$

which holds for a time function assumed zero outside the interval

$$0 \leqslant t \leqslant T$$

has a two-dimensional equivalent

$$\vec{S}(\vec{k}, \omega) = \vec{E}(\vec{k}, \omega) \times \vec{H}^*(\vec{k}, \omega) = \iint \langle \vec{E}(\vec{r}, \omega) \times \vec{H}^*(\vec{r} - \vec{\gamma}, \omega) \rangle_{\vec{R}} \, e^{i\vec{k}\cdot\vec{\gamma}} \, d\gamma_x d\gamma_y \tag{II-8}$$

and inverse transform

$$\langle \vec{E}(\vec{r}, \omega) \times \vec{H}^*(\vec{r} - \vec{\gamma}, \omega) \rangle_{\vec{R}} = \iint \vec{S}(\vec{k}, \omega) \, e^{-i\vec{k}\cdot\vec{\gamma}} \, \frac{dk_x dk_y}{(2\pi)^2} \tag{II-9}$$

where $\langle \; \rangle_T$ denotes a time average

$$\int_o^T \frac{\vec{E}(\vec{r}, t) \times \vec{H}(\vec{r}, t - \tau)}{T} \, dt \tag{II-10}$$

and $\langle \; \rangle_{\vec{R}}$ a spatial average. Thus, the power in the direction $\vec{k}$ is given by the two-dimensional transform of the spatial crosscorrelation function. The power in the direction $\vec{k}$ per unit solid angle and frequency interval is more commonly known in radio astronomy as the brightness distribution, while the spatial crosscorrelation is often known as the complex visibility function or "fringe" amplitude and phase. When two antennas are used to measure the spatial cross-correlation, the electric fields have been filtered by the antenna apertures. If the two antennas decompose the electric field vector into two orthogonal polarizations a and b, then

$$T_{a,b}(k_x, k_y, \omega) = \frac{\iint X_a(\omega) \, Y_b^*(\omega) \, e^{i\vec{k}\cdot\vec{\gamma}} \, d\gamma_x d\gamma_y}{\left\{ G_{x_a}(k_x, k_y, \omega) \, G_{y_b}^*(k_x, k_y, \omega) \right\}} \tag{II-11}$$

where $X(\omega)$ and $Y(\omega)$ are the Fourier components of the antenna outputs. $|G_x|^2$ and $|G_y|^2$ are the antenna power gains, and $\vec{\gamma}$ is the vector from the phase center of antenna Y to the phase center of antenna X. $T_{a,b}$ is the brightness temperature for the Stokes parameter a, b. $\vec{k} \cdot \vec{\gamma}/\omega$ is the delay which a signal wave vector $\vec{k}$ will undergo in reaching the phase center of antenna X. $|\vec{k}| \, \gamma_x/2\pi$ and $|\vec{k}| \, \gamma_y/2\pi$ are the projected baseline components in wavelengths which produce fringe spacing of $2\pi/|\vec{k}| \, \gamma_x$ and $2\pi/|\vec{k}| \, \gamma_y$ radians in the x and y directions. The sampling

theorem which is usually applied to band-limited functions can be applied to the complex visibility and its transform. When the source distribution is limited to $\pm\Theta_x$ and $\pm\Theta_y$, then the complex visibility function need only be sampled at integral multiples of $(2\Theta_x)^{-1}$ and $(2\Theta_y)^{-1}$ wavelengths.[5] Also, since the brightness temperature is real

$$[X_a(\omega)\, Y_b^*(\omega)]_{\gamma_x,\gamma_y} = [X_a(\omega)\, Y_b^*(\omega)]^*_{-\gamma_x,-\gamma_y} \tag{II-12}$$

so that only half the complex visibility plane has to be mapped.

In practice, it is not easy to sample the complex visibility plane, as it is physically difficult to move antennas; consequently, in many interferometers the only points on the complex visibility plane that can be sampled are those on the contour mapped out by the source motion. Sources with fixed right ascension and declination trace out an ellipse on the complex visibility plane – a portion of which will be inaccessible if the source is not circumpolar. If azimuth and elevation are used, coordinates refer to the Zenith $\hat{i}_Z$, North $\hat{i}_N$, and East $\hat{i}_E$, then

$$\vec{\gamma} = D \sin E_B \hat{i}_Z + D \cos E_B \sin A_B \hat{i}_E + D \cos E_B \cos A_B \hat{i}_N \tag{II-13}$$

$$\vec{k} = \frac{\omega}{c} \{\sin E_S \hat{i}_Z + \cos E_S \sin A_S \hat{i}_E + \cos E_S \cos A_S \hat{i}_N\} \tag{II-14}$$

where D is the baseline length, E_B and A_B are the elevation and azimuth of the baseline, and A_S and E_S are the apparent azimuth and elevation of the source. C is the velocity of light along the baseline. The axes of rotation on some antenna mounts do not intersect, so the baseline becomes dependent on the source position. In these cases, additional vectors have to be introduced. From Eqs. (II-13) and (II-14),

$$\vec{\gamma} \cdot \vec{k} = \omega \tau_{intf} = \frac{\omega D}{C} \{\sin E_B \sin E_S + \cos E_B \cos E_S \cos(A_S - A_B)\} \quad . \tag{II-15}$$

It is often more convenient to use coordinates centered on a reference position in the sky close to the source being studied, in which case

$$\vec{\gamma} \cdot \vec{k} = \omega \tau_{intf} = \frac{\omega D}{C} \{\sin \delta_B \sin \delta_S + \cos \delta_B \cos \delta_S \cos(L_S - L_B)\} \tag{II-16}$$

where L is the hour angle, and δ is the declination. In this coordinate system, k_x and k_y can be expressed to first order in terms of the angular displacements in Θ_x right ascension and Θ_y declination. The components of projected baseline in the direction of increasing right ascension and declination are γ_x and γ_y, where

$$\gamma_x = D \cos \delta_B \sin(L_S - L_B) \tag{II-17}$$

$$\gamma_y = D\{\sin \delta_B \cos \delta_S - \cos \delta_B \sin \delta_S \cos(L_S - L_B)\} \tag{II-18}$$

$$k_x = \frac{\omega}{C} \Theta_x \tag{II-19}$$

$$k_y = \frac{\omega}{C} \Theta_y \quad . \tag{II-20}$$

III. METHODS OF CROSSCORRELATION

Although the spectral visibility function $X_a(\omega)\, Y_b^*(\omega)$ can, in principle, be determined by Fourier analysis and cross multiplication at the signal frequency, in practice the signal band

is reduced to video by single- or multiple-frequency conversion stages. After mixing with a local oscillator of frequency ω_o and phase Θ, the Fourier components of the output are

$$x(\omega) = X(\omega + \omega_o)\, e^{-i\Theta} + X(\omega - \omega_o)\, e^{i\Theta} \quad . \tag{III-1}$$

Thus, for an upper-sideband system

$$X(\omega) = x(\omega - \omega_o)\, e^{i\Theta} \quad , \quad \omega > 0 \tag{III-2}$$

and

$$Y(\omega) = y(\omega - \omega_o)\, e^{i\Delta\omega_o t}\, e^{i\varphi} \quad , \quad \omega > 0 \tag{III-3}$$

if the receiver Y has local oscillator frequency $\omega_o + \Delta\omega_o$ and phase φ. Hence,

$$X(\omega)\, Y^*(\omega) = x(\omega - \omega_o)\, y^*(\omega - \omega_o)\, e^{-i\Delta\omega_o t}\, e^{i(\Theta - \varphi)} \quad , \quad \omega > 0 \quad . \tag{III-4}$$

In order to obtain the complex visibility function in a form referenced to coordinates fixed in the sky, it is necessary to take out the rapid phase changes caused by source motion

$$\begin{aligned} X(\omega)\, Y^*(\omega)\, e^{+i\vec{k}\cdot\vec{\gamma}} &= X(\omega)\, Y^*(\omega)\, e^{i\vec{k}_{ref}\cdot\vec{\gamma}}\, e^{i\vec{k}'\cdot\vec{\gamma}} \\ &= X(\omega)\, Y^*(\omega)\, e^{i\omega\tau_{ref}}\, e^{(i\omega/c)\Theta_x\gamma_x}\, e^{(i\omega/c)\Theta_y\gamma_y} \quad . \end{aligned} \tag{III-5}$$

The visibility function referenced to the sky, $A\, e^{i\Theta}$, can be decomposed into various frequency-dependent and independent terms

$$\begin{aligned} A\, e^{i\Theta} &= X(\omega)\, Y(\omega)^*\, e^{i\omega\tau_{ref}} \\ &= x(\omega - \omega_o)\, y^*(\omega - \omega_o)\, e^{i\omega_o\tau_{ref}}\, e^{i(\omega-\omega_o)\tau_{ref}}\, e^{-i\Delta\omega_o t}\, e^{i(\Theta-\varphi)} \end{aligned} \tag{III-6}$$

where

$\omega_o \dfrac{d\tau_{ref}}{dt}$ = the fringe rotation rate,

$(\omega - \omega_o)\, \tau_{ref}$ = the frequency dependent phase,

$\Delta\omega_o$ = the local oscillator frequency difference,

$(\Theta - \varphi)$ = the instrumental phase.

Equation (III-6) shows that it is possible to rotate the fringes by offsetting the local oscillators. τ_{ref} should also include constant delays or instrumental delays in the system, such as those in cables and IF amplifiers. The signals are filtered so that

$$x'(\omega - \omega_o) = x(\omega - \omega_o)\, B_x(\omega - \omega_o) \tag{III-7}$$

$$y'(\omega - \omega_o) = y(\omega - \omega_o)\, B_y(\omega - \omega_o) \tag{III-8}$$

where B_x and B_y are the Fourier transforms of the bandpass functions for the two receivers, so that

$$A\, e^{i\Theta} = x'(\omega - \omega_o)\, y^*(\omega - \omega_o)\, \frac{e^{i\omega_o \tau_{ref}}\, e^{i(\omega-\omega_o)\tau_{ref}}\, c^{-i\Delta\omega_o t}\, e^{i(\Theta-\varphi)}}{B_x(\omega - \omega_o)\, B_y^*(\omega - \omega_o)} \quad . \tag{III-9}$$

This may be computed directly from a Fourier analysis of the signals, provided the time variation of the phase is small over the period of Fourier analysis T. The cross-spectral function may also be estimated by crosscorrelation in time and subsequent transformation since

$$\{A\, e^{i\Theta}\} = \int_{-\alpha}^{+\alpha} \left\langle x'(t)\, y'(t - \tau_{ref} - \tau)\, \frac{e^{i\omega_o \tau_{ref}}\, e^{-i\Delta\omega_o t}\, e^{i(\Theta-\varphi)}}{B_x B_y^*} \right\rangle_T$$

$$\times\, e^{-i(\omega-\omega_o)\tau}\, d\tau\, w(\tau) \tag{III-10}$$

under the condition that $T \gg \alpha$. The visibility function has been averaged over frequency with an effective filter response

$$\int_{-\alpha}^{+\alpha} \cos \Delta\omega\tau\, w(\tau)\, d\tau \tag{III-11}$$

where $w(\tau)$ is the transform weighting function.

The time crosscorrelation technique is particularly easy to implement if the signals are first infinitely clipped so that when

$$\begin{aligned} y', x'(t) \geqslant 0 \quad & y'', x''(t) = 1 \\ < 0 \quad & y'', x''(t) = -1 \end{aligned} \tag{III-12}$$

in which case

$$\langle x'(t)\, y'(t - \tau)\rangle_T = [\langle x^{2\prime}(t)\rangle_T \langle y^{2\prime}(t)\rangle_T]^{1/2}$$

$$\times \sin\frac{\pi}{2} \langle x''(t)\, y''(t - \tau)\rangle_T \tag{III-13}$$†

from the theory of Van Vleck.[6] The time crosscorrelation can only be performed for time intervals over which

$$\left| \left\langle e^{i\omega_o \tau_{ref}(t)}\, e^{-i\Delta\omega_o t} \right\rangle_T \right| \approx 1 \quad . \tag{III-14}$$

However, the time crosscorrelations can be rotated and averaged before the Fourier transform is taken. In practice, the local oscillators are set to take out the linear portion of the fringe rotation and the rest of the rotation is taken out after crosscorrelation, i.e.,

$$\left\langle x'(t)\, y'(t - \tau_{ref} - \tau)\, e^{i\omega\tau_{ref}}\, c^{-i\Delta\omega_o t} \right\rangle_T = \sum_{t'} \left\langle x'(t)\, y'\left(t - \tau_{ref_{t'}} - \tau\right) \right\rangle_{t'}$$

$$\times\, e^{i\omega\tau_{ref}(t')}\, e^{-i\omega_o t'} \tag{III-15}$$

† x'' and y'' are normalized to unit energy for time T.

where t' is a discrete time midway through each crosscorrelation. An additional requirement for this scheme to work is that the change of τ_{rcf} from one period to the next is small enough that

$$\Delta\omega \, \Delta\tau_{ref} \ll \pi \quad . \tag{III-16}$$

IV. CALIBRATION OF AN INTERFEROMETER

The normal convention in interferometry is to state visibility functions normalized so that an unresolved point source has a fringe amplitude of unity. When this is the case, the brightness temperature distribution can be obtained from the normalized distribution (the transform of normalized fringe amplitude and the source flux)

$$T_N(\omega, \theta_x, \theta_y) = \iint A_n(\omega, \gamma_x, \gamma_y) \, e^{(i\omega/c)\theta_x\gamma_x} \, e^{(i\omega/c)\theta_y\gamma_y} \, d\gamma_x d\gamma_y \tag{IV-1}$$

$$T_B(\omega, \theta_x, \theta_y) = \frac{F(\omega) \, T_N(\omega, \theta_x, \theta_y)}{\int T_N d\Omega} \quad . \tag{IV-2}$$

There are many ways of obtaining the normalized visibility function, about the simplest of which is to make measurements with zero spacing, since

$$A_n(\omega, \gamma_x, \gamma_y) = \frac{A(\omega, \gamma_x, \gamma_y)}{A(\omega, 0, 0)} \tag{IV-3}$$

but it is seldom possible to do this when the antennas are fixed. Thus, a more complicated method of calibration has to be employed which uses the measurements made with the individual antennas. For a single antenna

$$T_A(\omega) = \frac{[x'(\omega - \omega_o) \, x'^*(\omega - \omega_o) - x'_{ref} \, x'^*_{ref}] \, T_S}{x'_{ref} \, x'^*_{ref}} \tag{IV-4}$$

where T_A is the system temperature, and x'_{ref} is the Fourier component of the video output on cold sky. From Eq.(III-13),

$$T_A(\omega) = \frac{S_n(\omega) \, T'_S - S_{n_{BP}}(\omega) \, T_S}{S_{n_{BP}}(\omega)} \tag{IV-5}$$

where S_n are the Fourier transforms of the clipped autocorrelation function

$$S_n(\omega) = \int \sin \frac{\pi}{2} \langle x''(t) \, x''(t - \tau) \rangle_T \, e^{-i\omega\tau} \, d\tau \, w(\tau)$$

and

$$T'_S = \frac{T_S \times \text{total noise power on source}}{\text{total noise power off source}} \quad . \tag{IV-6}$$

When the projected baseline is zero, the signals are perfectly correlated so that

$$x(\omega - \omega_o) = c_x \left[\sqrt{T_{A_x}(\omega)} \, S_x(\omega) + \sqrt{T_{S_x}} \, n_x(\omega) \right] \tag{IV-7}$$

$$y(\omega - \omega_o) = c_y \left[\sqrt{T_{A_y}(\omega)}\, S_y(\omega) + \sqrt{T_{S_y}}\, n_y(\omega) \right] \tag{IV-8}$$

where c_x, c_y are constants, and $s(\omega)$ and $n(\omega)$ are normalized so that they each have unit magnitude. From Eqs. (III-7) and (III-8),

$$A(\omega, 0, 0) = c_x c_y \sqrt{T_{A_x}(\omega)\, T_{A_y}(\omega)}$$

$$= \frac{\sqrt{(x_{ref} x^*_{ref})\,(y_{ref} y^*_{ref})}\, \sqrt{T_{A_x}(\omega)\, T_{A_y}(\omega)}}{\sqrt{T_{S_x} T_{S_y}}\, \sqrt{|B_x|^2\, |B_y|^2}} \tag{IV-9}$$

so that

$$A_n(\omega, \gamma_x, \gamma_y) = \frac{x'y'^*\, e^{i\omega_o \tau_{ref}}\, e^{i(\omega-\omega_o)\tau_{ref}}\, e^{-i\Delta\omega_o t}\, e^{i(\Theta-\varphi)}\, \sqrt{T_{S_x} T_{S_y}}\, \sqrt{B_x^2 B_y^2}}{B_x B_y^* \sqrt{T_{A_x} T_{A_y}}\, \sqrt{(x_{ref} x^*_{ref})\,(y_{ref} y^*_{ref})}} \tag{IV-10}$$

$$= \frac{S_{n_{xy}}(\omega)\, \sqrt{T'_{S_x} T'_{S_y}}\, \sqrt{B_x B_x^* B_y B_y^*}}{\sqrt{S_{n_{BP_x}}(\omega)\, S_{n_{BP_y}}(\omega)}\, \sqrt{T_{A_x}(\omega)\, T_{A_y}(\omega)}\, B_x B_y^*} \tag{IV-11}$$

for the clipped system, where

$$S_{n_{xy}}(\omega) = \int \sin\frac{\pi}{2} \left\langle x''(t)\, y''(t - \tau_{ref} - \tau)\, e^{i\omega_o \tau_{ref}}\, e^{-i\Delta\omega_o t}\, e^{i(\Theta-\varphi)} \right\rangle_T$$

$$\times\, e^{-i(\omega-\omega_o)\tau}\, d\tau\, w(\tau) \quad . \tag{IV-12}$$

V. NOISE ANALYSIS

The signals can be represented in the frequency domain by

$$x(\omega) = \sqrt{T_{A_x}(\omega)}\, S_x(\omega) + \sqrt{T_{S_x}}\, n_x(\omega) \tag{V-1}$$

$$y(\omega) = \sqrt{T_{A_y}(\omega)}\, S_y(\omega) + \sqrt{T_{S_y}}\, n_y(\omega) \tag{V-2}$$

where T_A and T_S are the antenna and system temperatures, respectively, and $\overline{|S(\omega)|^2}$ and $\overline{|n(\omega)|^2}$ are unity. If the signal and noise are both Gaussian, they have independent Gaussian components with probability distribution

$$p(z) = \frac{1}{\sqrt{\pi}}\, e^{-z^2} \tag{V-3}$$

where z = Re $S(\omega)$, Im $S(\omega)$, Re $n(\omega)$, Im $n(\omega)$ so that

$$\overline{x(\omega)\, x^*(\omega)} = T_{A_x}(\omega)\, \{\overline{[\mathrm{Re}\, S_x(\omega)]^2} + \overline{[\mathrm{Im}\, S_x(\omega)]^2}\}$$

$$+ T_{S_x}\, \{\overline{[\mathrm{Re}\, n_x(\omega)]^2} + \overline{[\mathrm{Im}\, n_x(\omega)]^2}\}$$

$$= T_{A_x}(\omega) + T_{S_x} \qquad \text{(V-4)}$$

while

$$\overline{[x(\omega)\, x^*(\omega)]^2} - \overline{[x(\omega)\, x^*(\omega)]}^2 = T_{A_x}^2(\omega)\, \{\overline{[\mathrm{Re}\, S_x(\omega)]^4} + \overline{[\mathrm{Im}\, S_x(\omega)]^4}$$

$$+ 2\, \overline{[\mathrm{Re}\, S_x(\omega)]^2}\, \overline{[\mathrm{Im}\, S_x(\omega)]^2}\} + T_{S_x}^2 \Big\{\overline{[\mathrm{Re}\, S_x(\omega)]^4}$$

$$+ \overline{[\mathrm{Im}\, n_x(\omega)]^4} - \Big[T_{A_x}(\omega) + T_{S_x}\Big]^2$$

$$+ 2\, \overline{[\mathrm{Re}\, S_x(\omega)]^2}\, \overline{[\mathrm{Im}\, n_x(\omega)]^2}\Big\}$$

$$+ 4 T_{A_x} T_{S_x}\, \{\overline{[\mathrm{Re}\, S_x(\omega)]^2}\, \overline{[\mathrm{Re}\, n_x(\omega)]^2} + \ldots\}$$

$$= \Big[T_{A_x}(\omega) + T_{S_x}\Big]^2 \qquad \text{(V-5)}$$

where the bar denotes the statistical or ensemble average. If an average is performed over frequency, then

$$\mathrm{Var}\, \langle x(\omega)\, x^*(\omega)\rangle_{\Delta\omega} = \frac{\Big(T_{A_x} + T_{S_x}\Big)^2}{\frac{\Delta\omega}{2\pi}\, \Delta t} \qquad \text{(V-6)}$$

since there are $(\Delta\omega/2\pi)\, \Delta t$ independent frequency Fourier components in the time interval Δt. The above result is the well-known noise in a total-power radiometer. Now, consider the cross spectrum multiplied by a factor of two so that the results can be compared with a total-power radiometer

$$2x(\omega)\, y^*(\omega) = 2\sqrt{T_{A_x}(\omega)\, T_{A_y}(\omega)}\, S_x(\omega)\, S_y^*(\omega) + 2\sqrt{T_{S_x} T_{S_y}}\, n_x(\omega)\, n_y^*(\omega)$$

$$+ 2\sqrt{T_{A_x}(\omega)\, T_{S_y}}\, S_x(\omega)\, n_y^*(\omega) + 2\sqrt{T_{A_y}(\omega)\, T_{S_x}}\, n_x(\omega)\, S_y^*(\omega) \quad . \qquad \text{(V-7)}$$

The first term is the signal and has a statistical average equal to twice the visibility function, while the uncorrelated portion of the first term and the other terms make up the noise. The first term can be considered as the vector

$$\vec{S} = 2\,\mathrm{Re}\sqrt{T_{A_x}(\omega)\,T_{A_y}(\omega)}\,S_x(\omega)\,S_y^*(\omega)\,\hat{i}_{Re} + 2\,\mathrm{Im}\sqrt{T_{A_x}(\omega)\,T_{A_y}(\omega)}\,S_x(\omega)\,S_y^*(\omega)\,\hat{i}_{Im} \quad . \tag{V-8}$$

In the case of a weak signal ($T_A \ll T_S$) perfectly correlated such as that from a point source, the noise vector is just

$$\vec{N} = 2\,\mathrm{Re}\sqrt{T_{S_x}T_{S_y}}\,n_x(\omega)\,n_y^*(\omega)\,\hat{i}_{Re} + 2\,\mathrm{Im}\sqrt{T_{S_x}T_{S_y}}\,n_x(\omega)\,n_y^*(\omega)\,\hat{i}_{Im} \quad . \tag{V-9}$$

The real and imaginary components are Gaussian random variable with zero mean and

$$\overline{\left[2\sqrt{T_{S_x}T_{S_y}}\,\mathrm{Re}\,n_x(\omega)\,n_y^*(\omega)\right]^2} = 4T_{S_x}T_{S_y}\{\overline{[\mathrm{Re}\,n_x(\omega)]^2}\;\overline{[\mathrm{Re}\,n_y(\omega)]^2} + \overline{(\mathrm{Im}\,n_x)^2}\;\overline{(\mathrm{Im}\,n_y)^2}\}$$

$$= 2T_{S_x}T_{S_y} \quad . \tag{V-10}$$

The real and imaginary components are independent since

$$\overline{\mathrm{Re}\,n_x n_y^*\,\mathrm{Im}\,n_x n_y^*} = \overline{(\mathrm{Re}\,n_x\,\mathrm{Re}\,n_y + \mathrm{Im}\,n_x\,\mathrm{Im}\,n_y)(-\mathrm{Re}\,n_x\,\mathrm{Im}\,n_y + \mathrm{Re}\,n_y\,\mathrm{Im}\,n_x)}$$

$$= 0 \tag{V-11}$$

using the property that

$$\overline{x_1x_2x_3x_4} = \overline{x_1x_2}\;\overline{x_3x_4} + \overline{x_1x_3}\;\overline{x_2x_4} + \overline{x_1x_4}\;\overline{x_2x_3} \tag{V-12}$$

for a Gaussian process. The probability distribution of the noise vector is

$$p(a,b) = \frac{1}{2\pi\sigma^2}\,e^{-(a^2+b^2)/2\sigma^2} \tag{V-13}$$

where

$$a = \vec{N}\cdot\hat{i}_{Re} \tag{V-14}$$

$$b = \vec{N}\cdot\hat{i}_{Im} \tag{V-15}$$

and

$$\sigma^2 = \frac{2T_{S_x}T_{S_y}}{\frac{\Delta\omega}{2\pi}\,\Delta t} \tag{V-16}$$

so that

$$p(|\vec{N}|) = \frac{|\vec{N}|}{\sigma^2} e^{-|\vec{N}|^2/2\sigma^2} \qquad |\vec{N}| \geq 0 \tag{V-17}$$

$$p(\Theta) = \frac{1}{2\pi} \qquad 0 \leq \Theta < 2\pi \quad . \tag{V-18}$$

The length of the noise vector is a Rayleigh distribution with mean $\sqrt{(\pi/2)}\,\sigma$ and $\overline{(|\vec{N}|^2)} = 2\sigma^2$, as shown in Fig. 1.

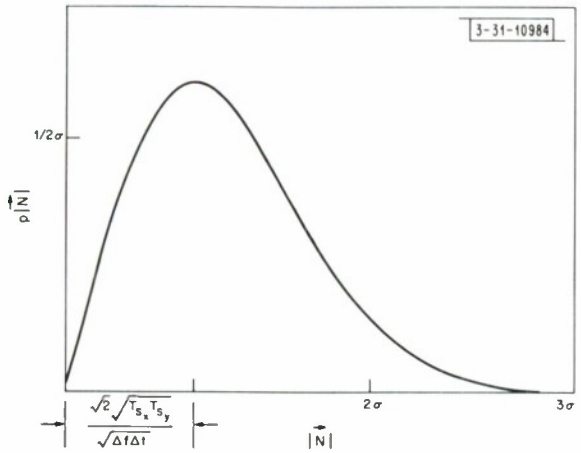

Fig. 1. Probability distribution of amplitude of noise vector.

The rms deviation of the amplitude A and phase φ of the visibility function estimate can be simply written only when the signal vector is much stronger than the noise vector, in which case

$$\overline{|\vec{S} + \vec{N}|} \approx |\vec{S}| \tag{V-19}$$

$$\overline{|\vec{S} + \vec{N}|^2} = |\vec{S}|^2 + \overline{|\vec{N}|^2} \tag{V-20}$$

and

$$\Delta A_{rms} = (\overline{|\vec{N}|^2})^{1/2} = \sqrt{2\sigma} = \frac{2\sqrt{T_{S_x} T_{S_y}}}{\sqrt{\frac{\Delta\omega}{2\pi}\,\Delta t}} \quad °K \tag{V-21}$$

$$\bar{A} = 2\sqrt{T_{A_x}(\omega)\, T_{A_y}(\omega)} \quad °K \text{ for point source} \tag{V-22}$$

and

$$\Delta\varphi_{rms} = \frac{\overline{|N|^2}\,\overline{\sin^2\Theta}}{\bar{A}^2} = \frac{\sigma}{\bar{A}} = \frac{\sqrt{2}\sqrt{T_{S_x} T_{S_y}}}{\bar{A}\sqrt{\frac{\Delta\omega}{2\pi}\,\Delta t}} \quad . \tag{V-23}$$

Expressions for intermediate signal levels have to be evaluated by integration. If the cross-correlation technique is applied to a single antenna, the signal vector reduces to $\sqrt{T_{A_x} T_{A_x}}$ since 3 dB is lost in splitting the power between receivers, while the rms noise is $\sigma = \sqrt{2}T_S/\sqrt{(\Delta\omega/2\pi)\,\Delta t}$ since only one component of noise affects the signal whose phase is fixed. The crosscorrelation receiver thus has $\sqrt{2}$ more noise than the total-power receiver, but yields the additional

information of receiver baseline subtraction. When an interferometer is used to measure the flux of a point source whose position in the fringe pattern is unknown, the signal-to-noise ratio is the same as that of a total-power radiometer of one antenna if both interferometric antennas and receiver systems have the same signal-to-noise ratios. In the preceding analysis, only the case of a point source and a high system-to-signal temperature ratio was considered. In the other extreme, when the normalized fringe amplitude is much smaller than unity, the magnitude of the signal vector is

$$2\sqrt{T_{A_x}(\omega)\, T_{A_y}(\omega)}\, |A_n| \tag{V-24}$$

and the rms noise $(|\vec{N}|^2)^{1/2}$ is

$$\frac{2\sqrt{\left[T_{A_x}(\omega) + T_{S_x}\right]\left[T_{A_y}(\omega) + T_{S_y}\right]}}{\sqrt{\frac{\Delta\omega}{2\pi}\,\Delta t}} \tag{V-25}$$

since the uncorrelated signals now effectively add to the system temperatures. This result can be seen by evaluating the cross terms of Eq. (V-7) which were previously neglected.

VI. SOURCE MODELS

Certain source distributions have very simple complex visibility functions. For example, a point source has a normalized visibility magnitude of unity and a phase

$$\frac{D\omega}{c}\left\{(\sin\delta_B \cos\delta_S)\,\Delta\delta_S + [\cos\delta_B \cos\delta_S \sin(L_S - L_B)]\,\Delta RA_S - [\cos\delta_B \sin\delta_S \cos(L_S - L_B)]\,\Delta\delta_S\right\} \tag{VI-1}$$

where ΔRA_S and $\Delta\delta_S$ are the position offsets of the source from the reference position. Even if only a small coverage of projected baseline is observable, it is generally possible to use a least-squares fitting technique to find the source position. If the signal-to-noise is good, no ambiguities are likely to arise in the fitting process, especially if the phase is tracked continuously so that only a small range of multiples of 2π need be tried in the fitting procedure. In general, the fitting process is better than taking the two-dimensional transform only over the range of projected baselines covered, owing to the restriction to a particular source model.

Other simple visibility functions are those of a circularly symmetric source whose phase is zero when refined to the source centroid, and a uniform disk source of radius R whose fringe amplitude is

$$\left|\frac{J_1\left(\frac{R}{S}\,2\pi\right)}{\frac{R\pi}{S}}\right|$$

where J_1 is the first-order Bessel function, and S is the fringe spacing or the reciprocal of the projected baseline length in wavelengths.

VII. INDEPENDENT TIME STANDARDS INTERFEROMETER

Recently, several interferometers have been operated with independent time and frequency standards at the two antennas, thereby eliminating the real-time link between the two antennas.

Coherent integration of the visibility function over a time T is possible if the spectral purity and stability of the two frequency standards are such that

$$|\langle e^{i\Delta\varphi(t)}\rangle_T| \approx 1 \qquad \text{(VII-1)}$$

where $\Delta\varphi(t)$ is the phase difference between the two local oscillators after removal of any constant frequency difference by a frequeney offset search. For a rubidium-controlled crystal clock (a crystal clock which is phase locked to a rubidium line), coherent integration times, for a system at 1666 MHz, of a few minutes are possible. For a resolution bandwidth of Δf, the maximum allowable time error $\Delta\tau$ must be such that

$$\Delta f \Delta\tau \ll 1 \quad . \qquad \text{(VII-2)}$$

Time synchronization close enough for an initial signal detection can, in practice, be achieved using Loran time transmissions. A fringe frequency and time error search can be performed by computing the visibility funetions for short-time intervals with sufficient frequeney resolution to account for any delay errors (or equivalently taking enough points in the crosscorrelation function to ensure reaching the real zero point), and then coherently averaging the visibility funetion to maximize the amplitude and minimize the phase shift across the band.

Stated mathematically, the frequency offset and delay are determined by maximizing

$$\left| \sum_{t'} \sum_{\omega} A_{t'}(\omega)\, e^{i\Theta_{t'}(\omega)}\, e^{iFt}\, e^{i\tau\omega} \right| \qquad \text{(VII-3)}$$

where $A_{t'}(\omega)\, e^{i\Theta_{t'}(\omega)}$ is the complex fringe amplitude determined over a short period centered at t'. τ and F are the delay and frequency search parameters, which may be quantized provided

$$|\langle e^{i(\Delta F t/2\pi)}\rangle_T| \approx 1 \qquad \text{(VII-4)}$$

and $\Delta\tau\Delta\omega \ll \pi$. The delay search is more conveniently performed in the time domain by searching the delay shift of the crosscorrelation function.

For a continuum source, the cross spectral function of the video signals is

$$A\, e^{i\Theta}\, e^{2\pi i F_R t}\, e^{i\omega\tau_{intf}}\, e^{i\omega\tau_e}\, e^{-i\omega\tau_{st}} \qquad \text{(VII-5)}$$

for the single-sideband system and

$$A\cos(\Theta + 2\pi F_R t)\, e^{i\omega\tau_{intf}}\, e^{i\omega\tau_e}\, e^{-i\omega\tau_{st}} \qquad \text{(VII-6)}$$

for a double-sideband system, where A and Θ are fringe amplitude and phase, F_R is the fringe rate, τ_{intf} is the geometric interferometer delay, and τ_e is a timing error. τ_{st} is the tape time shift necessary to take out τ_{intf}. The double-sideband system has the disadvantage of requiring a least-squares fitting procedure owing to the lack of a quadrature component, but has the advantage of timing errors not affecting the fringe phase. The Fourier transform of (VII-5) is

$$R_{xy}(\tau) = \langle x(t)\, y(t-\tau)\rangle = 2A\cos(\Theta + 2\pi F_R t)\, g_1(\tau + \tau_{intf} + \tau_e - \tau_{st})$$
$$- 2A\sin(\Theta + 2\pi F_R t)\, g_2(\tau + \tau_{intf} + \tau_e - \tau_{st}) \qquad \text{(VII-7)}$$

where

$$g_1(\tau) = \int_0^{\omega_{max}} \cos \omega\tau \, \frac{d\omega}{2\pi} = \frac{\sin \omega_{max}\tau}{2\pi\tau} \tag{VII-8}$$

and

$$g_2(\tau) = \int_0^{\omega_{max}} \sin \omega\tau \, \frac{d\omega}{2\pi} = \frac{1 - \cos \omega_{max}\tau}{2\pi\tau} \tag{VII-9}$$

while the transform of (VII-6) is

$$R_{xy}(\tau) = A \cos(\theta + 2\pi F_R t) \, g_1(\tau + \tau_{intf} + \tau_e - \tau_{st}) \quad . \tag{VII-10}$$

The fringe rate F_R includes both the source motion and the oscillator offsets and is sufficiently slow that immediate crosscorrelation may be performed. Additional rotation and delay are introduced in the fringe rate and delay search as in Eq. (VII-3), as often as is required to ensure no significant reduction in fringe amplitude.

The interval T over which

$$| \langle e^{i\Delta\varphi(t)} \rangle_T | \approx 1 \tag{VII-11}$$

is the maximum coherent integration period possible without significant reduction in fringe amplitude. After the limit of coherent integration has been reached, it is still possible to improve the knowledge of the fringe amplitude with incoherent averaging. The incoherent average

$$\left\{ \sum_{i=0}^{N} \frac{|A_i|^2}{N} \right\} \tag{VII-12}$$

yields no phase information and cannot be used for position measurements or to obtain a brightness distribution, but the magnitude will still indicate the effective source size. The signal-to-noise ratio that can be obtained with incoherent averaging approaches that of the Hanbury Brown and Twiss interferometer in the limit when the bandwidth of the coherent integration BW approaches the bandwidth of signals before crosscorrelation – in other words, when the coherent integration time reduces to the reciprocal of the pre-crosscorrelation bandwidth.

For a spectral line source, the noise analysis is:

$$\overline{\left\{ \sum_{0}^{N} \frac{|A_i|^2}{N} \right\}} = \overline{\left\{ \sum_{0}^{N} \frac{|\vec{S}|^2 + |\vec{N}|^2}{N} \right\}} = 4T_{A_x}(\omega) \, T_{A_y}(\omega) + 4 \, \frac{T_{S_x} T_{S_y}}{(\Delta\omega/2\pi)\,\Delta t} \tag{VII-13}$$

from Eqs. (V-20) and (V-21). For small signals,

$$\sqrt{\overline{\left\{ \sum_{0}^{N} \frac{|A|^2}{N} \right\}^2} - \overline{\left\{ \sum_{0}^{N} \frac{|A|^2}{N} \right\}}^2} = \sqrt{\frac{\overline{|\vec{N}|^4}}{N}} = \frac{4\sqrt{2} T_{S_x} T_{S_y}}{\sqrt{N}\,[(\Delta\omega/2\pi)\,\Delta t]} \quad . \tag{VII-14}$$

If BW is defined as the reciprocal of Δt, and τ as the total integration time, then Eq. (VII-14) becomes

$$\frac{4\sqrt{2}T_{S_x}T_{S_y}}{\sqrt{(\Delta\omega/2\pi)\,\tau}\,[\sqrt{(\Delta\omega/2\pi)}/\sqrt{BW}]} \qquad \text{(VII-15)}$$

and the signal-to-noise ratio is

$$\left(\frac{T_{A_x}T_{A_y}}{T_{S_x}T_{S_y}}\right)\frac{\sqrt{(\Delta\omega/2\pi)\,\tau}\,\sqrt{\Delta\omega/2\pi}}{\sqrt{2BW}} \quad .$$

When the source being observed has spectral features, it is possible to coherently average the data using one of the strong features as a phase calibration. This method can effectively make the interferometer phase stable when the signal-to-noise ratio is good on the calibration feature. However, the eomplex visibility functions are now no longer referred to the sky, and a map relative to the ealibration feature will be obtained. For this averaging process,

$$A = \sum_{0}^{N} \frac{A_n e^{-i\varphi_{neal}}}{N}$$

where φ_{neal} is the phase of the calibration feature for the n^{th} coherent integration period. This proeess has no effeet on the interferometer noise provided the ealibration feature has negligible noise. Another possible teehnique for removing differential phase noise due to drifting standards is to simultaneously observe a strong calibration souree with another set of antennas or off-axis feed system. If the ealibration source is strong enough to produce a phase with little noise in the coherent integration period, these phases ean then be used to increase coherent integration time on the souree being examined. Of eourse, the different position of the calibrator would have to be taken into aecount in obtaining the phase correction term. This technique could also be used to remove the atmospherie distortion which limits optical astronomy. For example, if a ealibration star is sufficiently close to the objeet of interest, say, a planet, the fringe pattern will be jittering in the same fashion on the planet as it does on the star; eonsequently, it should be possible by electronie image superposition to integrate the visibility functions coherently. The phase ehange due to the atmosphere to the first order for a plane parallel atmosphere is

$$\frac{\omega}{e}\left\{\int_0^L (n(\ell)-1)\,d\ell - \int_0^{L'} (n(\ell')-1)\,d\ell'\right\} \qquad \text{(VII-16)}$$

where ℓ and ℓ' are the paths through the atmosphere. Typieally, the atmosphere adds about 20 cm to the path and, owing to turbulenee, the path will not be the same for the two apertures of the interferometer. This differential phase fluctuation whieh is given by the above equation is not serious at radio frequeneies below about 3 GHz as it seldom reaches 90° peak, even for widely separated antennas. However, at optieal frequencies, it is signifieant for paths separated by only a few eentimeters. An approximate angular distance over which the differential phase fluctuations will remain highly correlated is the diameter of an aperture over which phase deviations are smaller than π divided by the length of the atmosphere where most fluctuations oeeur. In the optieal range, this is only about 20 seeonds of are, but this is still large compared with the resolution; eonsequently, the use of a phase ealibrator within 20 seconds of the object of interest eould be used to take out atmospherie fluetuations. At 8 GHz, a phase ealibrator within 30 minutes of are would probably suffiee.

VIII. HAYSTACK-MILLSTONE INTERFEROMETER

The 120-foot antenna of the Haystack Microwave Research Facility and the 84-foot antenna of the Millstone Radar Facility, both operated by Lincoln Laboratory, were used as an interferometer. The antennas are separated by approximately 2250 feet along a line approximately 19° East of North. This baseline gives a minimum fringe spacing of 54 seconds of arc at 18 cm and provides a good range of projected baseline for a wide range of declination. The convenient baseline and the spectral processing equipment at Haystack make the system ideal for a study of OH emission regions that were unresolved with a single antenna. Figure 2 shows the projected baseline coverage for the OH emission sources.

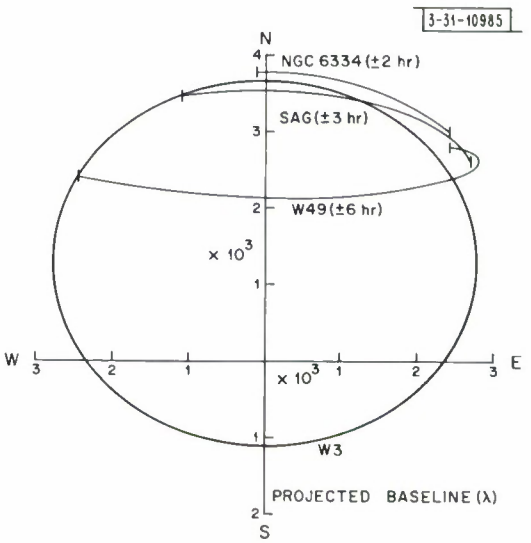

Fig. 2. Fringe amplitude phase coveroge for some OH sources. Limits shown are observoble limits.

A block diagram of the Millstone receiver front end is shown in Fig. 3. Circular and linear polarization is obtained from a dual-mode horn whose output ports give vertical and horizontal polarization. Combining vertical and horizontal signals through a hybrid complex gives left- and right-circular polarization after correct adjustment of the phase lengths. The antenna output is amplified by a tunnel diode amplifier and then filtered to reject the image band. A ferrite switch is included for calibration measurements. In the normal interferometer mode, the switch remains switched to the antenna side. A noise source is used for single-antenna and system-temperature measurements.

The local oscillator signal is derived by phase locking an oscillator to the sum or difference of a harmonic of 67 MHz and a signal whose frequency could be varied approximately 28 MHz. For the OH emission measurements, the 24^{th} harmonic was selected. The output of the oscillator was filtered to attenuate any spurious signals that tend to be produced by the synchronizer. Figure 4 is a block diagram of the local oscillator system.

The mixer output is amplified by a 30-MHz amplifier with a 10-MHz bandwidth. A line driver then boosts the level to 100 mW. The Haystack receiver front end did not require the line driver, owing to its proximity to the control room where the IF outputs are combined. Otherwise, the Haystack front end is similar to that at Millstone.

The intersite coupling of the radiometers involves the transmission of antenna-pointing commands to Millstone, remote control of the radiometer, transmission of the intermediate

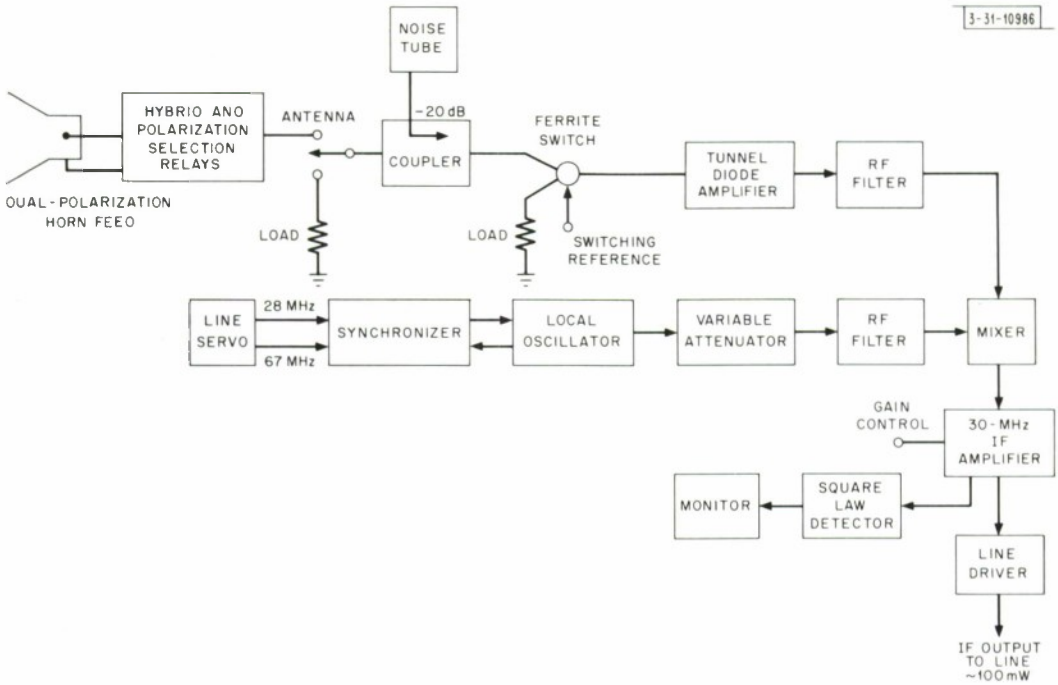

Fig. 3. Radio frequency section of Millstone receiver.

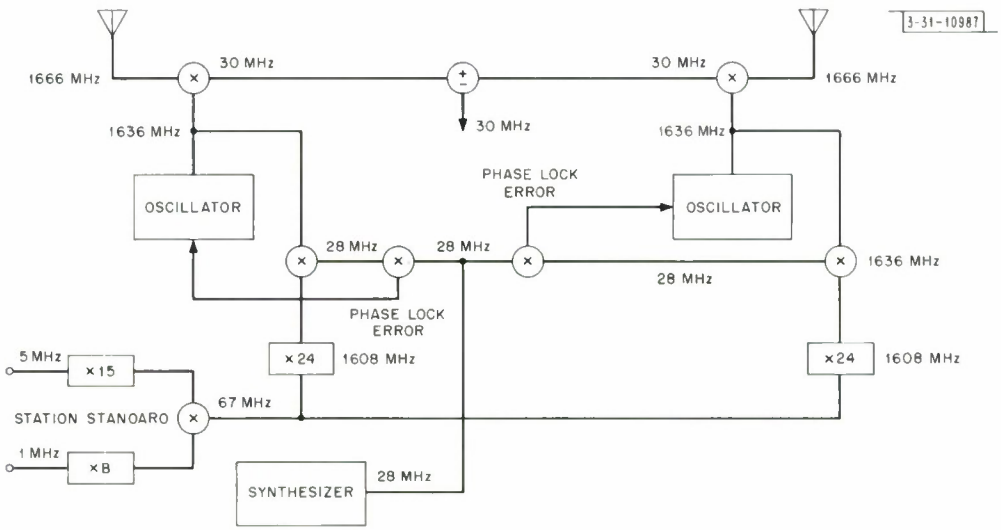

Fig. 4. Local oscillator system shown for center of band at 1666 MHz.

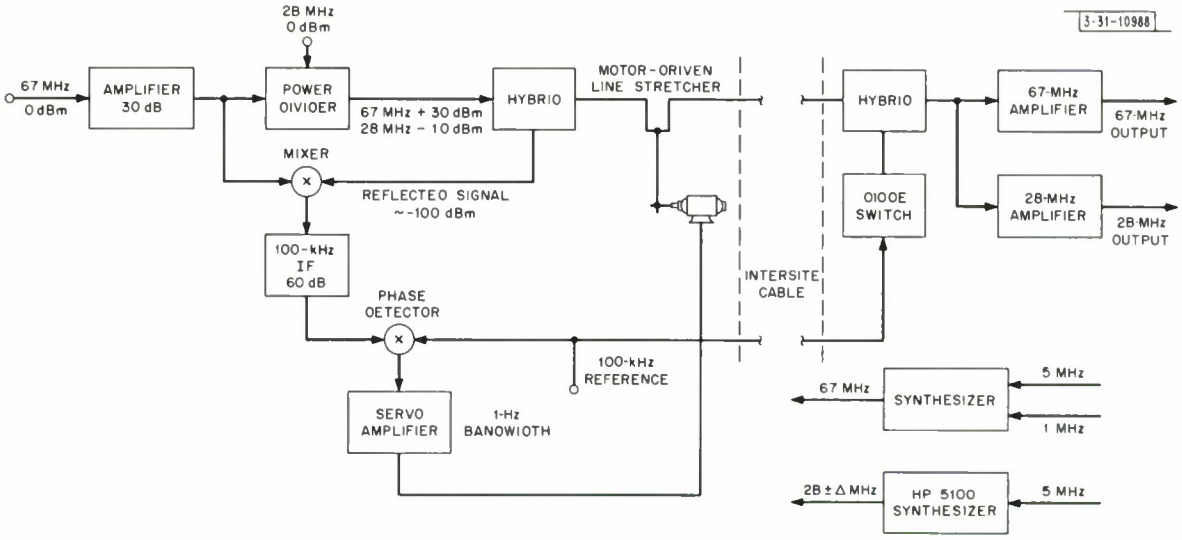

Fig. 5. Line servo to maintain phase stability.

frequency to Haystack, and two-way coupling of the local oscillator reference signals. To maintain good phase stability, the reference signals are transmitted along a servo-controlled line that nullifies line length changes caused by temperature change and other effects. The transmission system also has to overcome a large line attenuation of 55 dB for one-way transmission at 67 MHz. The selection of a lower basic frequency would have reduced attenuation, but would have made phase locking to L-band more difficult. A block diagram of the line servo is shown in Fig. 5. The 67-MHz reference signal is amplified to approximately 1 watt and transmitted to the line through a hybrid junction. At the receiving end of the line, a portion of the signal is reflected. The reflected signal undergoes phase reversal with a 100-kHz rate as the diode switch modulates the reflection coefficient from $+\frac{1}{2}$ to $-\frac{1}{2}$. Very little of the 100-MHz modulation is passed into the 67-MHz amplifier because of the isolation afforded by the hybrid tee. At the transmitting end, the reflected signal is mixed with the 67-MHz reference signal and amplified. The output of the 100-kHz amplifier is proportional to $\cos\varphi \cos 2\pi ft$, where f = 100 kHz, and φ is the phase of the 67-MHz signal after having traveled twice the line length. Multiplication of this signal by the 100-kHz reference signal produces the necessary error signal from the servo loop. The high loop gain makes it possible for the line servo to maintain a constant electrical line length to within a small fraction of an inch.

The IF signals are either added or subtracted, as shown in Fig. 6. The combined signal is filtered and converted to video. The autocorrelation function of the clipped and sampled video signal is taken with a digital correlator.

The difference of the autocorrelation functions for the added and subtracted signals yields the real part of the crosscorrelation function since

$$[x(t) + y(t)]\,[x(t-\tau) + y(t-\tau)] - [x(t) - y(t)]\,[x(t-\tau) - y(t-\tau)]$$
$$= 2x(t)\,y(t-\tau) + 2y(t)\,x(t-\tau) \qquad \text{(VIII-1)}$$

and

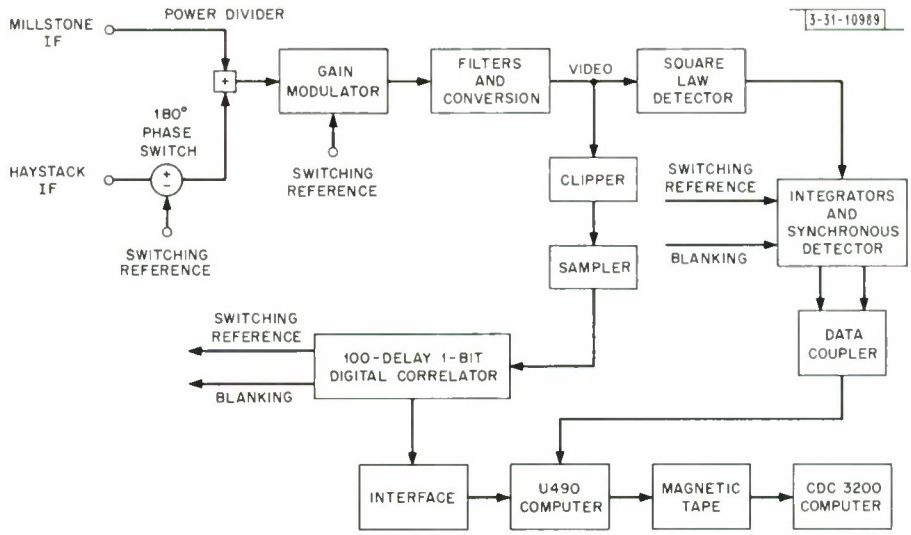

Fig. 6. Crosscarrelotian scheme by addition ond subtraction of IF signols.

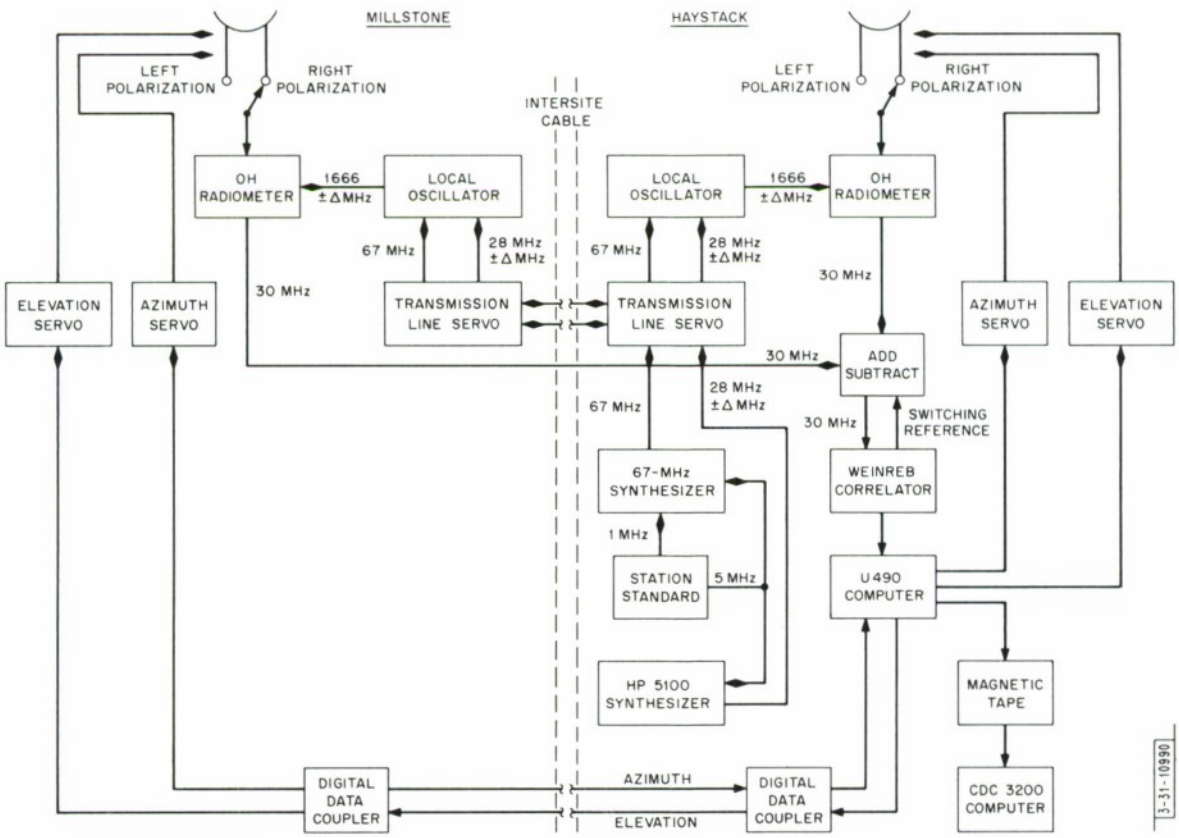

Fig. 7. Hoystock-Millstane interferometer.

$$2 \int [\langle x(t)\, y(t-\tau)\rangle_T + \langle y(t)\, x(t-\tau)\rangle_T]\, e^{-i\omega\tau}\, d\tau$$

$$= 4\ \mathrm{Re}\ x(\omega)\, y^*(\omega)$$

$$= 4\ \mathrm{Re}\ A\, e^{-i\omega\tau_{ref}(t)} \quad . \qquad \text{(VIII-2)}$$

The real and imaginary components of the complex visibility function can be found by a least-squares fitting. This system yields an effective system temperature of

$$\sqrt{T_{S_x} T_{S_y}}$$

if the signal powers are added with equal power. However, the noise level is twice that of direct crosscorrelation.

Autocorrelation functions of the sum and difference signals are transferred alternately to a computer every 100 msec. The basic correlation period is 87.5 msec. The system is blanked for 12.5 msec while the data are being transferred to the U490 computer. Signal bandwidths of 4 MHz, 1.2 MHz, 400 kHz, 120 kHz, and 40 kHz can be analyzed by selecting appropriate filter and sampling frequencies. The autocorrelation function is a 16-bit binary word for each of 100 delays. An extra bit is used to indicate the state of the switching reference signal. The autocorrelation functions, together with continuum data, bandwidth and correlator mode, and antenna command azimuth and elevation, are transferred to magnetic tape. A block diagram of the whole system is shown in Fig. 7.

Single-antenna measurements were made to measure the aperture efficiencies. The antenna temperatures of Cassiopeia A were 160° and 180°K, which indicated efficiencies of 40 and 25 percent for the Millstone and Haystack antennas, respectively.

After the individual radiometers were examined for linearity, bandpass, and lack of spurious signals, the system was checked for phase coherence and phase stability. The test arrangement is illustrated in Fig. 8. A signal from a test oscillator is connected to each radiometer individually and then simultaneously. When the oscillator is swept in frequency, the bandpass is displayed when only one radiometer is connected to the oscillator. When both radiometers are

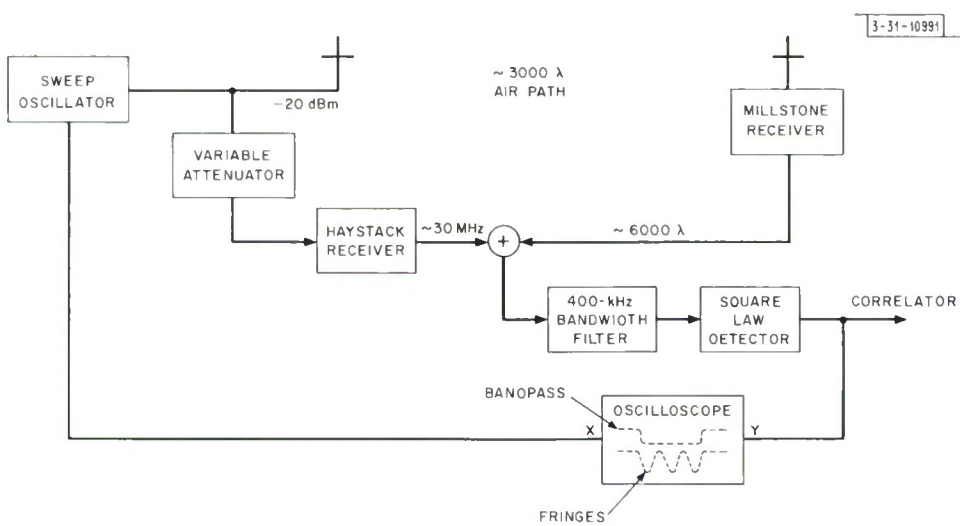

Fig. 8. Interferometer test system.

swept simultaneously, fringes appear because of the phase relationship between the radiometer outputs. The fringe spacing in Hertz is the reciprocal of the delay in seconds. Measurements of the fringe pattern and bandpass functions showed that the phase noise in the system produced less than 2-percent reduction in fringe amplitudes. The phase stability was better than 50° during 24 hours. Some of this shift may have been due to the measuring technique, as observations of continuum radio sources indicated better stability.

The trombone section of the line servo was observed to move approximately 5 feet during the sunrise and sunset period when the temperature changed about 50°F.

IX. WIDE EFFECTIVE BANDWIDTH INTERFEROMETER

When an independent standards long-baseline interferometer is used to measure the positions of unresolved continuum point sources, the phase information is seldom usable since it is not possible to calibrate the phase at time intervals sufficiently frequent to ensure its constancy. Consequently, the position must be obtained by least-squares fitting the fringe rate F_R to obtain the offsets in right ascension and declination. From Eq. (II-16),

$$F_R = \frac{d\omega\tau_{intf}}{dt} = -\frac{\omega D}{c}\frac{dL_S}{dt}\cos\delta_B\cos\delta_S\sin(L_S - L_B) \tag{IX-1}$$

and, hence,

$$\Delta F_R = \frac{\omega D}{c}\frac{dL_S}{dt}\cos\delta_B\,[\Delta\delta_S\sin\delta_S\sin(L_S - L_B) + \Delta RA_S\cos\delta_S\cos(L_S - L_B)] \quad . \tag{IX-2}$$

If, however, the delay can also be precisely measured, then least-squares fitting to the delay difference $\Delta\tau_{intf}$ yields more information on the source offsets. From Eq. (II-16),

$$\Delta\tau_{intf} = \frac{D}{c}\{(\sin\delta_B\cos\delta_S)\,\Delta\delta_S + [\cos\delta_B\cos\delta_S\sin(L_S - L_B)]\,\Delta RA_S - [\cos\delta_B\sin\delta_S\cos(L_S - L_B)]\,\Delta\delta_S\} \quad . \tag{IX-3}$$

Like the fringe-rate fitting, the delay does not have the ambiguity difficulties that fringe-phase fitting presents. In fact, one measurement of fringe and delay gives the source position offset. Fringe-rate fitting yields an offset resolution of

$$\frac{\lambda}{D}\left[\frac{\Delta F_R}{2\pi(dL_S/dt)}\right] \tag{IX-4}$$

or, if the fringe rate can be measured to 1 cycle per hour, the offsets can be measured to approximately 24 times the fringe spacing. Delay fitting yields an offset resolution of

$$\frac{\lambda_o}{D}\left(\Delta\tau\,\frac{\omega_o}{2\pi}\right) \tag{IX-5}$$

where λ_o and $\omega_o/2\pi$ are some "center" wavelength and frequency. For example, measurements of delay to 1 nsec would yield an offset resolution of twice the fringe spacing for a 2-GHz center-frequency system.

In practice, measurement of delay between two very long baseline interferometer stations would not require recording a very large bandwidth, as the signal can be sampled at various

small-bandwidth windows within a large bandwidth. Extrapolation of the fringe phase from one window to the next could provide an increasingly precise delay measurement.

Measurement of delay and fringe rate with a very long baseline interferometer would provide an extremely precise technique for measurement of the positions of radio sources; then, reversing the previous analysis would provide a precise technique for measurement of positions on the earth's surface as well as irregularities in the earth's rotation.

X. SUMMARY AND CONCLUSIONS

In Sec. II, we discussed the principles of interferometry, or how the angular distribution of electromagnetic radiation is related to the electric field at certain "sample" points. While an antenna samples and adds the electric field at many points by virtue of its structure or geometry, a two-element interferometer samples the single antenna "filtered" electric field at only two points instantaneously, but can build up many sample points as the baseline changes in time. Since all the sample points are not merely added but crosscorrelated, the resultant antenna can be imagined to be electrically steered by the phase term in the two-dimensional transform.

The noise analysis of Sec. V shows the relation of the noise in the fringe amplitude and phase to the noise levels of the individual systems. It is interesting to note that, while an interferometer can map an area within the single-antenna beam with a signal-to-noise ratio of a single antenna, a super large parabolic antenna (diameter approximately that of the maximum interferometer baseline) used to map the same region does not gain in signal-to-noise ratio by the ratio of its area to the single-dish area. This is because the super large dish has to be mechanically scanned over the region; hence, the effective integration time is reduced by the ratio of its beam area to the map area. Thus, an interferometer uses the collecting area efficiently, like a multiple-feed antenna or camera with photographic emulsion.

Although this report mainly discusses spectral line interferometry or the mapping of frequency dependent brightness distributions, the section on wide effective bandwidth interferometry (Sec. IX) can be alternately viewed as using the wide bandwidth to increase the number of sample points in the complex visibility plane when the source distribution remains constant with frequency.

Because very large antenna structures are not mechanically feasible, interferometry has become a very important technique for high resolution source mapping and point source position measurements. Very long baseline interferometers have application for clock synchronization, antenna site position measurement, and numerous geophysical experiments as well as astronomical measurements.

ACKNOWLEDGMENTS

The author is grateful to the numerous people who contributed to this work. The Haystack-Millstone interferometer was constructed and operated with help from J. M. Moran, P. P. Crowther, J. A. Ball, G. M. Hyde, V. C. Pineo, J. C. Carter, R. H. Erickson, R. Lewis, and D. C. Papa. The author is also indebted to Professors A. H. Barrett and B. F. Burke who provided the impetus for the interferometer experiment from which most of the theory in this report was derived.

REFERENCES

1. A. H. Barrett, IEEE Trans. Military Electron. MIL-8, 156 (1964).
2. A. E. E. Rogers, et al., Astrophys. J. 147, 369 (1967), DDC 649278.
3. J. M. Moran, et al., Astrophys. J. 148, L69 (1967), DDC 652914.
4. J. M. Moran, et al., Science 157, 676 (1967), DDC 661152.
5. R. N. Bracewell, Proc. IRE 46, 97 (1958).
6. J. H. Van Vleck and D. Middleton, Proc. IEEE 54, 2 (1966).

DOCUMENT CONTROL DATA – R&D

(Security classification of title, body of abstract and indexing annotation must be entered when the overall report is classified)

1. ORIGINATING ACTIVITY *(Corporate author)* Lincoln Laboratory, M.I.T.	2a. REPORT SECURITY CLASSIFICATION Unclassified 2b. GROUP None

3. REPORT TITLE

Spectral Line Interferometry and Interferometer Noise Analysis

4. DESCRIPTIVE NOTES *(Type of report and inclusive dates)*

Technical Report

5. AUTHOR(S) *(Last name, first name, initial)*

Rogers, Alan E.E.

6. REPORT DATE	7a. TOTAL NO. OF PAGES	7b. NO. OF REFS
16 January 1968	28	6

8a. CONTRACT OR GRANT NO.	9a. ORIGINATOR'S REPORT NUMBER(S)
AF 19(628)-5167 b. PROJECT NO. 649L c. d.	Technical Report 441 9b. OTHER REPORT NO(S) *(Any other numbers that may be assigned this report)* ESD-TR-67-595

10. AVAILABILITY/LIMITATION NOTICES

This document has been approved for public release and sale; its distribution is unlimited.

11. SUPPLEMENTARY NOTES	12. SPONSORING MILITARY ACTIVITY
None	Air Force Systems Command, USAF

13. ABSTRACT

The theory of spectral line interferometry is developed with special reference to interferometer systems built to study the emission from interstellar OH molecules. Expressions for the root-mean-square noise of visibility amplitude and phase are derived in terms of the geometric means of the system and antenna temperatures. Methods are discussed for obtaining the visibility function from measurements made at widely separated sites by means of precise frequency and time standards.

14. KEY WORDS

interferometers
interferometry
spectral lines
noise
Haystack
Millstone
correlation techniques